PCCP

Accepted Manuscript

ROYAL SOCIETY OF CHEMISTRY

www.rsc.org/pccp

Journal Name

ARTICLE

Influence of relative humidity on heterogeneous kinetics of NO_2 on kaolin and hematite

Received 00th January 20xx,
Accepted 00th January 20xx

DOI: 10.1039/x0xx00000x

www.rsc.org/

Yongchun Liu, Chong Han, Jinzhu Ma, Xiaolei Bao and Hong He*

In order to obtain a reliable kinetic parameter, it is required to measure the reaction kinetics for the important heterogeneous reactions at ambient relative humidity (RH). In this study, the uptake coefficients and HONO yields were measured at RH from 7 % to 74 % and at ambient pressure in the dark for the heterogeneous reaction of NO_2 on kaolin and hematite using a coated-wall flow tube reactor. The initial true uptake coefficient ($\gamma_{t,ini}$) of NO_2 at RH 7% was measured to be (1.44±0.10) $\times10^{-7}$ and (1.58±0.13) $\times10^{-6}$ on kaolin and hematite, respectively, while it decreased notably on both minerals accompanied by an increase of HONO yields as RH increased. The average $\gamma_{t,ini}$ at RH 32 %-74 % was (4.42±1.17) $\times10^{-8}$ and (2.83±0.84) $\times10^{-7}$ on kaolin and hematite, respectively. The corresponding mean HONO yield was (36.0±16.1) % and (75.9±3.32) %, respectively.

Introduction

In the past decades, due to the possible roles in atmospheric chemistry, considerable attention has been paid to heterogeneous reactions between nitrogen oxides (NO_x) and atmospheric particulate matter (APM), including soot [1-4], mineral dust [5-8] and sea salts [9, 10]. For example, heterogeneous reactions of NO_x on soot and mineral dust can produce gaseous HONO [3, 4, 11], which is a daytime source of OH radical [12]; while reactions between NO_x and sea salts might be a source of Cl radical [10]. Mineral dust is an important component of APM, with a loading of 1000-3000 Tg/yr [13]. Model results indicate that interactions of N_2O_5, O_3 and HO_2 radical with dust can affect the photochemical oxidant cycle, causing O_3 decreases up to 10 % in and nearby the dust source areas [13]. The presence of dust could also result in a decrease in concentrations of SO_2, NO_y (NO_3+N_2O_3+HNO_3), H_xO_y (OH+HO_2+H_2O_2) through heterogeneous reactions by 10.3 %-52.5 %, 16.0 %-99.7 %, and 11.3 %-59.4 %, respectively, under typical dust storm conditions [14]. In addition, it has been found that heterogeneous chemistry including SO_2 and NOx on dust plays a significant role in regional haze formation in China [15-17].

Uptake coefficients (γ) is one of the key parameters in modeling studies. Several studies have measured the γ of NO_2 on dust from Saharan or Asian source regions [5, 18] and on surrogate materials including $CaCO_3$ [7], Al_2O_3, Fe_2O_3, CaO, MgO, TiO_2 [5, 19] and clay minerals [6]. The γ of NO_2 on these samples varies from 10^{-4} to 10^{-9} depending on the substrates and experimental conditions [20], and it was recommended to be 1.2×10^{-8} by Crowley et al.[21]. Except for a few reaction systems, such as reactions of NO_2 on TiO_2 [18, 22, 23], Saharan sand [23],and $CaCO_3$ [7], however, most of these γ values were measured under dry condition due to the limitation of low pressure reactors used [5, 19] or at a single point of relative humidity (RH = 25 %, for NO_2 on TiO_2 and Saharan sand, the γ was measured) [18, 23]. However, γ has been found to show a strong dependence on humidity for some reactions. Both increases and decreases of γ have been observed as a function RH [7,22, 24, 25]. Recently, it has been found that heterogeneous uptake of NO_2 on soil [26] and montmorillonite [27] was depressed notably by water.

In the recent work [16], the revised Community Multi-scale Air Quality Model (CMAQ) with simple heterogeneous chemistry greatly minimized the gaps between the model and observation results, while relative large errors still remained. This means more refined kinetic parameters for the relevant reactions are required to further improve the model performance. In the real troposphere, RH typically varies from 20 % to 90 %. Thus, the quantitatively dependence of γ on RH needs to be investigated case by case for these important heterogeneous reactions [28]. At present date, the RH dependent γ of NO_2 on kaolin and hematite are unavailable for current modeling simulation.

The reactive process of NO_2 on dust is regarded as an initial adsorption and reaction of NO_2 with the surface oxides followed by secondary processes, or heterogeneous hydrolysis of NO_2 to yield HONO and HNO_3 [20]. Besides surface nitrates and nitrites [19, 29-31], HONO is also detected as a gaseous product [6, 11, 18]. Under ultra violet irradiation, the HONO yield (γ_{HONO}) is 75 %, 33 % and 80 % for reactions of NO_2 on pure TiO_2 [22], 1% TiO_2/SiO_2 and Sahara sand [18], respectively. It has been postulated that surface acidity, microstructure and other unclear factors control the production of HONO [18]. However, it is unclear yet about the

State Key Joint Laboratory of Environment Simulation and Pollution Control, Research Center for Eco-Environmental Sciences, Chinese Academy of Sciences, Beijing, 100085, China. E-mail: honghe@rcees.ac.cn

† Electronic Supplementary Information (ESI) available: [Diagram of the flow tube; Evolution of NO concentrations with time during uptake of NO_2 on kaolin and hematite; Comparison of the uptake curves of NO_2 with or without Na_2CO_3 denuder; The relative ratio of NO_2 removed by Na_2CO_3 denuder to the initial NO2 concentration at different RH; Linear mass dependence for uptake capacity of NO_2 within 30 min on kaolin and hematite]. See DOI: 10.1039/x0xx00000x

HONO yields for heterogeneous reactions of NO_2 on kaolin and hematite; and it is also unknown that how the RH affects HONO yield for reactions of NO_2 on them.

In this study, kaolin and hematite, which are identified as the mineralogical composition of dust samples [32], were used as a proxy of mineral dust to investigate the effect of RH on kinetics and HONO yields for reactions with NO_2. The uptake experiments were carried out at ambient RH and at ambient pressure using a flow tube reactor. The quantitative dependence of uptake coefficients and HONO yields with RH on kaolin and hematite was obtained. The environmental implications were also discussed.

Experimental section

Materials. Hematite (AR) was from Beijing Nanshang Chemicals Factory. Kaolin was supplied by Huaibei Junteng Kaolinite Co., Ltd and originated from Anhui province, China. The mineralogy was confirmed by X-ray diffraction (XRD) analysis (D/max-RB). The specific surface area for hematite and kaolin was 2.7 $m^2 \cdot g^{-1}$ and 12.4 $m^2 \cdot g^{-1}$, respectively, measured by nitrogen Brunauer-Emmett-Teller (BET) physisorption analyzer (Quantachrome Autosorb-1-C). NO_2 standard gas (50 ppmv in N_2, Beijing Huayuan Gases Inc.), and high purity of N_2 and O_2 (99.99%, Beijing AP BEIFEN Gases Inc.) were used as received.

Experimental Methods. The experiments were performed in a 20 cm×1.0 cm (i.d.) horizontal cylindrical coated-wall flow tube reactor (Figure S1), which has been described detailedly elsewhere [33] and is similar to that used by Ndour et al. [23]. The temperature was maintained at 298 K by circulating water through the outer jacket of the flow tube reactor. Simulated air was used as carrier gas, and the total flow introduced in the flow tube reactor was 770 $ml \cdot min^{-1}$, ensuring a laminar regime at ambient pressure. NO_2 was introduced into the flow tube through a movable injector with 0.3 cm radius. NO_2 concentration was (150±5) ppb and was measured using a NO_x analyzer (THERMO 42i). A Na_2CO_3 denuder tube (10 cm × 1.0 cm i.d.) was introduced between the exit of the flow tube reactor and the detector to trap the formed HONO since it is also detected as NO_2 by the analyzer [18]. Thus, HONO concentration was indirectly measured as the difference of the detected signals with and without the Na_2CO_3 denuder in the sampling line. This method has been verified in our previous work [33]. RH was adjusted by the ratio of dry N_2 to wet N_2 and measured by a hygrometer (Center 314). Powder samples were suspended in ethanol and dripped uniformly into the Pyrex flow tube and dried overnight in an oven at 393 K. It has been confirmed that the adsorption of reactant gases on the quartz tube is negligible in blank experiments.

The kinetics was reported in terms of uptake coefficient, which was proportional to the measured first-order rate constant derived from the uptake curves when the Na_2CO_3 denuder was used, k_{obs}, as following Equation[18, 33].

$$k_{obs} = \frac{\gamma_{obs} < c >}{2r_{tube}} \quad (1)$$

Where r_{tube}, γ_{obs} and <c> are the flow tube radius, the geometric uptake coefficient and the average molecular velocity of NO_2, respectively. A correction for gas phase diffusion limitations was taken into account for γ_{obs} calculations using Cooney-Kim-Davis (CKD) method [34, 35]. Then, the true uptake coefficient (γ_t) was obtained from the mass-dependence of γ_{obs} as follows [25],

$$\gamma_t = [slope] \frac{A_g}{S_{BET}} \quad (2)$$

where [*slope*] is the slope of the plot of γ_{obs} versus sample mass in the linear regime (mg^{-1}); A_g is the inner surface area of the sample tube (cm^2); and S_{BET} is the specific surface area of the particle sample ($cm^2 \cdot mg^{-1}$).

Results and discussion

Figure 1 shows the typical uptake curves of NO_2 on kaolin and hematite as well as the corresponding evolution of the γ_{obs} with time. The black lines and the red ones show the data collected with 10 s and 1 min of time resolution, respectively. As shown in Figures 1A and B, once the kaolin or hematite sample was exposed to NO_2, a large initial NO_2 uptake was observed and followed by a quick recovery. After 20 min, a stable consumption of NO_2 was observed on both kaolin and hematite. The c/c_0 (20-30 min) was (0.869±0.005) and (0.902±0.006) for these two specific experiments, respectively. This steady uptake of NO_2 was always observed for all uptake experiments at different RH, which implies occurrence of catalytic reaction. When the samples were isolated from reactant gas by moving the injector outside the reaction region, only a small amount of NO_2 (<4 %) desorbed from both kaolin and hematite. This means reactive uptake should mainly contribute to the uptake of NO_2 on these samples.

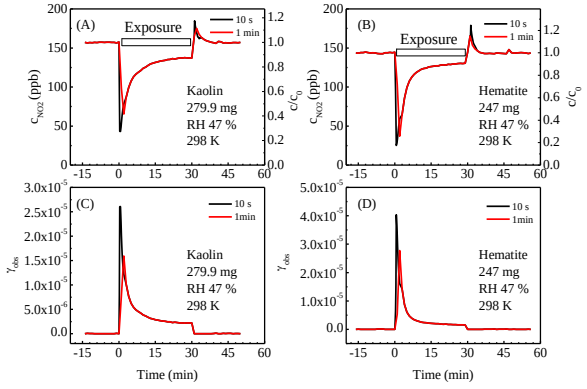

Figure 1. Uptake curves of NO_2 on (A) 279.9 mg kaolin and (B) 247 mg hematite; and evolution of the observed uptake coefficient on (C) 279.9 mg kaolin and (D) 247 mg hematite at 298 K and at 47 % of RH.

Because NO is thermodynamically balanced with NO_2, ~3 % NO always presented in the reactant gas. Figure S2 shows the evolution of NO concentrations with time during uptake of NO_2 on kaolin and hematite at RH of 47 % and 7 %, respectively. Within the instrument uncertainty, NO concentrations did not change during uptake experiments on hematite at all of the tested relative humidity (7%-74%). Uptake of NO on kaolin, however, was observed clearly at RH 7 %, which suggests adsorption of NO onto kaolin. This phenomenon is opposite to that observed by Underwood et al. [19] using a Knudsen cell-mass

spectrometer, in which NO was observed as the predominant gas phase product for the reaction of NO_2 with mineral oxides. This might result from different reaction conditions, such as mineral oxides, RH, concentration and pressure. In our work, high concentration of O_2 (20 %) should be favourable to NO oxidation, but be unfavourable to NO_2 dissociation on the surface. On the other hand, RH in this study is much higher than that in Underwood's work [19]. A higher RH may be favourable to heterogeneous hydrolysis of NO_2.

Using infrared spectroscopy, surface species including nitrates and nitrites have been well characterized for heterogeneous reactions of NO_2 on mineral oxides [19, 29, 30, 36, 37] as well as kaolin [6]. The surface nitrogen with oxidation state of +5, +4 and +3 were also confirmed using X-ray spectroscopy [31]. Additionally, gas phase HNO_3, NO, and HONO were detected [6, 19]. Based on these previous work [19, 30, 38], following reactions were summarized as the possible reaction pathways in the dark.

$MO^- + NO_2(g) \rightleftharpoons MO\text{-}NO_2^-(ads)$ (3)

$MO+2NO_2(ads) \rightleftharpoons MO\text{-}N_2O_4(ads) \rightleftharpoons MO\text{-}NO^+NO_3^-(ads)$ (4)

$MO\text{-}NO_2^-(ads)+NO_2(g) \rightarrow MO\text{-}NO_3^-(ads)+NO(g)$ (5)

$2MO\text{-}NO_2^-(ads) \rightarrow MO^- + MO\text{-}NO_3^-(ads) + NO(g)$ (6)

$M\text{-}O^- + NO_2(g) \rightarrow M\text{-}NO_3^-(ads)$ (7)

$2M\text{-}O^- + N_2O_4(ads) \rightarrow MO\text{-}NO_2^-(ads) + MO\text{-}NO_3^-(ads)$ (8)

$MO\text{-}NO_2^-(ads) + MO\text{-}H_2O(ads) \rightarrow MO\text{-}OH(ads) + MO^- + HONO(g)$ (9)

$M\text{-}OH + NO_2(g) \rightarrow M\text{-}O + HONO(g)$ (10)

$2NO_2(g) + MO\text{-}H_2O(ads) \rightarrow MO\text{-}HNO_3(ads) + HONO(g)$ (11)

$2M\text{-}OH + 2NO_2(g) \rightarrow MO\text{-}NO_3^-(ads) + MO\text{-}NO_2^-(ads) + MO\text{-}H_2O(ads)$ (12)

The reactions (3), (5), (7), and (10)-(12) should contribute to the loss of NO_2 from gas phase during uptake experiments. The reactions (5), (6), and (9)-(11) involving in release of gas phase NO and HONO should be responsible for the uptake of NO_2 at steady state after the surface species is saturated. However, as shown in Figure 2S, release of NO was not observed on both kaolin and hematite under all of the tested RH (7 %-47 %). This means that the reactions (5) and (6) should be a minor reaction pathway under our reaction conditions, although they cannot be ruled out yet owing to adsorption or reactions in gas phase or on the surface. Thus, the uptake at steady state should be mainly related to these reactions involving in HONO formation. The contribution of reactions (9)-(11) to NO_2 uptake and HONO formation will be discussed later.

Figures 1C and D shows the evolution of the γ_{obs} with reaction time. The γ_{obs} decreased quickly with reaction time due to the surface saturation by surface species mentioned above. Thus, time resolution showed a great effect on the uptake coefficient. For example, in these two specific experiments shown in Figure 1, the γ_{obs}(10 s) is 2.61×10^{-5} (279.9 mg kaolin) and 4.03×10^{-5} (247 mg hematite) at 298 K and RH 47 %, while the corresponding γ_{obs}(1 min) is 1.59×10^{-5} and 2.78×10^{-5}, respectively. The γ_{obs}(SS) at steady state (20-30 min) decreased to $(2.28\pm0.10)\times10^{-6}$ and $(1.69\pm0.10)\times10^{-6}$, respectively, with a decreasing amplitude of one order. Therefore, three values for γ_{obs}, that's, γ_{obs}(10 s), γ_{obs}(1 min) and γ_{obs}(SS) were reported here.

As mentioned in Experiment Section, gas phase diffusion was corrected for γ_{obs} calculations using Cooney-Kim-Davis (CKD) method [34, 35]. In the coated-wall flow tube reactor, powder samples with multilayers were usually generated. In order to determine the probe depth of NO_2 in the multilayers samples, the response of γ_{obs} with sample mass were measured. Figure 2 shows the typical linear mass dependence of γ_{obs} on kaolin and hematite. Thus, the true uptake coefficient (γ_t, BET) can be obtained using Equation 2. The γ_t(10 s), γ_t(1 min) and γ_t(SS) of NO_2 on kaolin at RH 47 % are $(4.85\pm0.39)\times10^{-8}$, $(3.46\pm0.25)\times10^{-8}$, and $(3.74\pm0.27)\times10^{-9}$, respectively. They are $(3.23\pm0.23)\times10^{-7}$, $(1.89\pm0.18)\times10^{-7}$, and $(1.50\pm0.05)\times10^{-8}$, respectively, on hematite. The corresponding values of γ_t(10 s), γ_t(1 min) and γ_t(SS) at other relative humidity were summarized in Table 1.

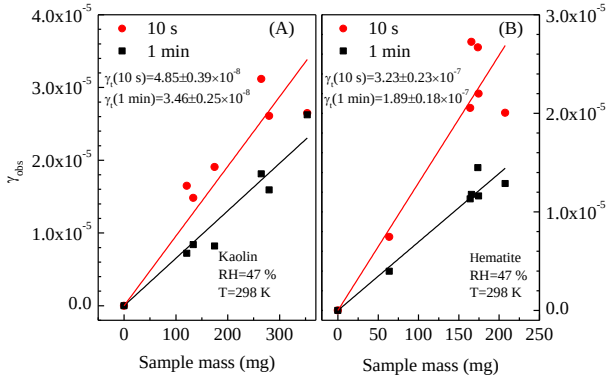

Figure 2. Linear mass dependence for γ_{obs} on (A) kaolin and (B) hematite at 298 K and at 47 % of RH.

Table 1. Summary of the measured γ_t and the y_{HONO} for the y_{HONO} for the heterogeneous reaction of NO_2 on kaolin and hematite at 298 K

RH %	Kaolin				Hematite			
	$\gamma_{t,ini}$(10s) ($\times10^8$)	$\gamma_{t,ini}$(1min) ($\times10^8$)	$\gamma_{t,ss}$ ($\times10^9$)	y_{HONO} (%)	$\gamma_{t,ini}$(10s) ($\times10^7$)	$\gamma_{t,ini}$(1 min) ($\times10^7$)	$\gamma_{t,ss}$ ($\times10^8$)	y_{HONO} (%)
7	14.4±0.01	8.69±0.01	4.56±0.15	3.4±2.4	15.8±1.30	13.5±1.30	1.24±0.18	19.4±0.4
15	8.93±0.39	3.89±0.15	3.04±0.16	9.0±2.9	7.37±0.35	5.46±0.50	1.31±0.07	39.1±1.6
32	5.32±0.21	3.30±0.15	2.56±0.01	18.0±0.8	3.40±0.33	2.06±0.19	1.31±0.06	72.1±3.9
47	4.85±0.39	3.46±0.25	3.74±0.27	41.0±2.2	3.23±0.23	1.89±0.18	1.50±0.05	78.2±1.6
74	3.10±0.14	2.03±0.29	4.26±0.06	49.4±2.8	1.86±0.07	1.16±0.08	1.23±0.06	77.4±0.1

As shown in Table 1, both kaolin and hematite showed the largest γ_t of NO_2 at RH 7 %. The γ_t(10 s) was (1.44±0.10) ×10^{-7} on kaolin, and it was (1.58±0.13) ×10^{-6} on hematite at RH 7 %. Figure 3 shows the dependence of γ_t of NO_2 on kaolin and hematite on RH. The γ_t(10s) decreased exponentially as RH increased. The experienced equations are,

on kaolin,

$$\gamma_t(10\ \mathrm{s}) = [(1.55 \pm 0.30) \times 10^{-7}]\exp[-\mathrm{RH}/(17.02 \pm 3.69)] + [(2.98 \pm 0.39) \times 10^{-8}] \quad (13)$$

on hematite,

$$\gamma_t(10\ \mathrm{s}) = [(1.83 \pm 0.76) \times 10^{-6}]\exp[-\mathrm{RH}/(13.63 \pm 5.22)] + [(1.83 \pm 0.30) \times 10^{-7}] \quad (14)$$

Thus, the γ_t(10 s) at RH of 0 % can be extrapolated from the above equations and are (1.85±0.34) ×10^{-7} and (2.01±0.79) ×10^{-6} on kaolin and hematite, respectively. The γ_t(10 s) values reported here are in the ranges of the γ_t from (8.1 ± 0.2) ×10^{-8} to (2.3 ± 0.4) ×10^{-7} for NO_2 on kaolin [6], and from 7 ×10^{-7} to 7.7 ×10^{-6} for NO_2 on hematite under dry condition [5, 19], respectively. At high RH (32 %-74 %), the average γ_t(10 s) of NO_2 on kaolin was (4.42±1.17) ×10^{-8}, and it was (2.83 ± 0.84) ×10^{-7} on hematite. It decreased by a factors of ~3, and ~9 on kaolin and hematite, respectively, when compared with the γ_t(10 s) at RH 0%. The influence of water on the γ of NO_2 on hematite and kaolin is similar to that on soil [26], while is slightly different from that on montmorillonite [27].

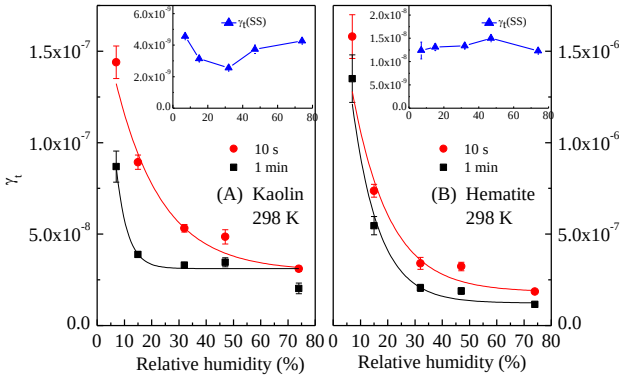

Figure 3. Dependence of the γ_t of NO_2 on the relative humidity. (A) kaolin and (B) hematite. The insert graph shows the corresponding γ_t(SS).

It has been well recognized that a higher concentration of reactant gas should lead to a smaller initial uptake coefficient owing to the surface saturation effect [18]. As the same reason and as illustrated in Figure 1, a larger initial uptake coefficient should be obtained at a shorter exposure time. It should be pointed out that the reactors and reaction conditions in these works related to NO_2 uptake are quite different. For example, Angelini et al. [6] measured the γ_t at RH 0 % and at NO_2 partial pressure from 2.3 ×10^{-4} to 3.6 ×10^{-3} mbar using a DRIFTS, and Underwood et al. [5, 19] carried out the experiments at RH 0 % and at NO_2 partial pressure from 5.3 ×10^{-6} to 10^{-2} mbar with a Knudsen cell reactor. In our work, the NO_2 partial pressure is 1.6 ×10^{-4} mbar at ambient pressure, and the lowest RH was 7 %. The concentration of NO_2 in this work (1.6 ×10^{-4} mbar) was slightly lower than that used by Angelini et al. [6], while it was higher than Underwood's [5]. Additionally, in DRIFTS experiments, the data collected within the first several minutes were usually used to calculate the uptake coefficients, whereas the time resolution of a Knudsen cell-mass spectrometer was often higher than 1 s. Thus, a lower time resolution should be achieved in Angelini's work [6], while a higher time resolution was in Underwood's work [5, 19]. Therefore, the γ_t(10 s) of NO_2 at RH 0% estimated in this work is larger than Angelini's results (8.1±0.2×10^{-8} at 2.3×10^{-4} mbar) on kaolin [6], while it is smaller than that of Underwood's results (7.7×10^{-6} at 5.3×10^{-6} mbar) on hematite [5].

As shown in Figure 3, besides the γ_t(10 s), the γ_t(1 min) of NO_2 also decreases with RH on kaolin and hematite. In particular, the curves in the low RH regions (<20 %) are much steeper than those in the high RH regions. The declination of the initial γ with RH can be ascribed to competitive adsorption between H_2O and NO_2, like the competitive adsorption of O_3, NO_2 or COS with H_2O on mineral oxides [22, 24, 25]. It has been found that a monolayer of H_2O on kaolin achieves at RH 13 % [6], and it does at RH 10 % on hematite [24]. The initial γ of H_2O on mineral dust (4.2±0.7×10^{-2}) [39] is much larger than that of NO_2 as discussed above. It means that adsorption of H_2O is preferred to NO_2 when the RH is lower than the RH of monolayer of water. This well explains the quick decrease of the initial γ_t of NO_2 in the low RH range. In addition, the γ_t(1 min) is more sensitive to RH than that of γ_t(10 s) in the low RH range because the longer exposure time is favourable to formation of a monolayer water. However, as shown in the insert graphs in Figure 3, the γ_t(SS) was not so sensitive to RH on hematite, while a decrease followed by an increase with RH was observed on kaolin.

HONO formation and HONO yields. Besides surface nitrites [19, 29, 30, 36, 37], HONO(g) was qualitatively confirmed during heterogeneous reaction of NO_2 on SiO_2 [11] and kaolin [6] using UV spectroscopy. Using a Long Path Absorption Photometer (LOPAP) [20] or NO_x analyzer [18, 22, 23], the yields of HONO were also measured directly or indirectly for the photochemical reaction of NO_2 on TiO_2 and Saharan sand [18, 22, 23]. The formation of HONO can be explained by the reactions (9)-(11). In fact, when the reaction (3) and the dissociation reaction of H_2O to form surface OH group are coupled with the reactions (9) and (10), a catalytic cycle from NO_2(g) to HONO(g) can be realized by the reaction of surface OH group as following. Thus, reactions (9)-(11) can be regarded as catalytic reactions.

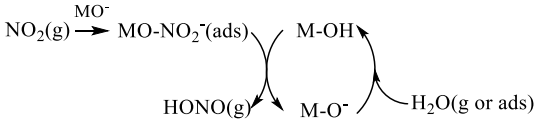

(15)

In above experiments, a Na_2CO_3 denuder between the outlet of the reactor and the NO_x analyzer was used to trap the formed HONO. In order to investigate the HONO yields, uptake experiments without Na_2CO_3 denuder were performed at RH 7 %-74 %. Figure S3 shows the comparison of the typical uptake curves of NO_2 on kaolin and hematite at RH 47% with or without Na_2CO_3 denuder. As can be seen from this figure, uptake capacity for NO_2 with a Na_2CO_3 denuder was clearly larger than that without a Na_2CO_3 denuder on both kaolin and hematite. Thus, the difference between them represents the amount of HONO formed during reaction. It should be pointed out that

Na_2CO_3 denuder can adsorb a small amount of NO_2 (2.8±0.8% regardless of RH, Figure S4). This difference might also partly result from gaseous reaction between NO_2 and H_2O. However, in the experiments with a Na_2CO_3 denuder, adsorption of NO_2 or HONO from gaseous reaction was saturated or subtracted before the samples were exposed to NO_2 gas. Therefore, the difference between uptake curves with and without Na_2CO_3 denuder strongly supports the formation of HONO during reactions of NO_2 on kaolin and hematite, and represents the net production of HONO from heterogeneous reaction.

In the uptake experiments, uptake curves of NO_2 on different sample mass were independently measured. As discussed above, uptake capacity linearly depends on sample mass in a wide mass range (Figure S5). Thus, through dividing the uptake capacity by the sample mass, the normalized differentiate uptake capacity with or without Na_2CO_3 denuder was obtained and shown in Figure 4. The error bars in Figure 4A and B represent the standard deviation (σ) for 5-7 independent experiments. The averaged differentiate uptake capacity of NO_2 with Na_2CO_3 denuder is clearly higher than that without Na_2CO_3 denuder on both kaolin and hematite. Figure 4C and D shows the evolution of HONO yield with reaction time. The error bars were calculated in the light of error propagation.

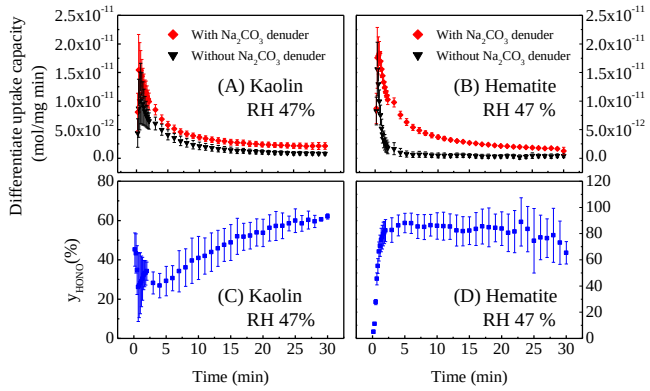

Figure 4. Evolution of the (A) and (B) uptake capacity of NO_2, and (C) and (D) HONO yield with time.

On kaolin, the initial y_{HONO} was around 30 %, and then gradually increased to 60 %, while it increased quickly from 5 % to 85 % within 3 min on hematite. These results indicate that the reactions (3), (5) and (7), which lead to surface nitrates and nitrites, mainly contribute to the initial uptake of NO_2 on either kaolin or hematite. This also well explains the quick deactivation for uptake NO_2 on kaolin and hematite (Figure 1). However, at steady state, uptake of NO_2 should be mainly ascribed to the reactions (9)-(11). Angelini et al. [6] proposed that reaction (9) might be related to HONO formation on kaolin because nitrites were not detected using both IR (at 1235 cm^{-1}) and ion chromatography. However, the reactions (10) and (11) cannot be ruled out yet because a non-zero initial HONO yield was observed on kaolin (shown in Figure 4C). In particular, the y_{HONO} on kaolin is around 50 % at steady state, which implies the importance of the disproportionation reaction (reaction 11) in HONO formation on kaolin. On hematite, however, a very small initial y_{HONO} (5 %) and a larger y_{HONO} at steady state (>50 %) indicate that the reactions (9) and (10) should be the main pathway for HONO formation. The accumulation of surface nitrites should explain the quick increase of y_{HONO} with time (Figure 4D). Therefore, these results imply different mechanism of HONO formation on different dust samples.

Figure S5 shows the linear dependence of integral uptake capacity on sample mass within 30 min. The slopes of these lines represent the integral uptake capacity of unit sample mass. For example, at 47 % RH, the slope was (1.09±0.07) $\times10^{-10}$ mol·mg^{-1} with Na_2CO_3 denuder on kaolin, while it was (6.40±0.19) $\times10^{-11}$ mol·mg^{-1} when a Na_2CO_3 denuder was not used. For hematite, the corresponding slope was (1.03±0.04) $\times10^{-10}$ mol·mg^{-1} and (2.25±0.24) $\times10^{-11}$ mol·mg^{-1}. Therefore, using these values, the integral HONO yield was calculated and summarized in Table 1. The influence of RH on integral uptake capacity and y_{HONO} are shown in Figure 5.

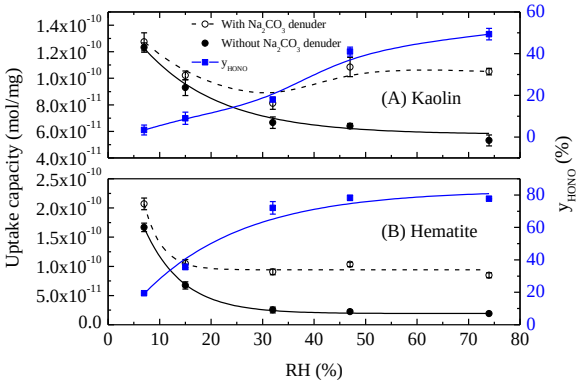

Figure 5. Evolution of integral uptake capacity and HONO yield within 30 min with RH on (A) kaolin and (B) Hematite. The lines are guides for the eye.

As shown in Figure 5, if a Na_2CO_3 denuder was not used, the integral uptake capacity of both kaolin and hematite to NO_2 gradually decreased with RH within 30 min, whereas different responses of the integral uptake capacity to RH were observed between these two minerals when a Na_2CO_3 denuder was used. On hematite, from RH 7 % to 15 %, the integral uptake capacity decreased by about one factor owing to competitive adsorption and it did not change any more with further increase in RH (the dot line). However, the integral uptake capacity on kaolin decreased with RH from 7 % to 32 %, and then increased with further increase in RH. This change trend was also observed for its γ_t(SS) as shown in Figure 3. It should be noted that kaolin consists of neutral layers containing one octahedral aluminium hydroxide sheet bonded to one tetrahedral silicon oxide sheet through a plane of shared oxygen atoms [6]. Although kaolin has a low shrink-swell capacity compared to montmorillonite, it slightly swells with increased water adsorption [40] should make more reactive sites (M-O or M-OH) available. Thus, increase of γ_t(SS) and the integral uptake capacity were observed when the RH was higher than 32 %. This is similar to the reaction of HNO_3 on Na-montmorillonite, on which the γ increases clearly at higher RH [41]. As shown in Figure 5 and Table 1, the integral HONO yield within 30 min increased from (3.4±2.4) % to

(49.4±2.8) % on kaolin, and it was from (19.4±0.4) % to (77.4±0.1) % on hematite when the RH increased from 7 % to 74 %. As discussed above, the values of the integral y_{HONO} also suggest that the reaction (11) (disproportionate reaction with a HONO yield of 50 %) should be the main mechanism for HONO formation on kaolin at high RH, while the reactions (9) and (10) (with a HONO yield of 100 %) should be important for HONO formation on hematite when the RH was larger than 32 %.

It should be pointed out that HONO from gas-phase reaction between NO_2 and H_2O at high RH might result in a positive bias for the measured heterogeneous HONO yields. However, this effect should be negligible in this study due to the following reasons. Firstly, we have measured the difference between the initial NO_2 concentrations with and without Na_2CO_3 denuder at different RH. If gas phase reaction significantly contribute to the monitored HONO signal, the fraction of the removed HONO (measured as NO_2 and formed in gas phase reaction) by Na_2CO_3 denuder should positively response to RH. However, as shown in Figure S4, the relative ratio of NO_2 removed by the Na_2CO_3 denuder to the initial NO_2 concentration was constant (2.8 ±0.8%) regardless of the RH value. Secondly, if gas phase reaction significantly contribute to the monitored HONO signal, a non-zero intercept should be expected when linearly fitting the uptake coefficient or the integral uptake capacity to sample mass at a fixed RH value because the converted NO_2 to HONO in gas phase should be a non-zero constant under the same residence time, NO_2 concentration and RH. However, as shown in Figures 2 and S5, both the uptake coefficient and the integral uptake capacity were linearly related to the sample mass with zero intercepts in spite of the RH values and sample types. Therefore, we are confident with that the measured HONO yield was related to heterogeneous reactions on these samples.

Conclusions and Atmospheric implications

Under dry condition, the $\gamma_{t,ini}$ of NO_2 on kaolin and hematite was (1.85±0.34) $\times10^{-7}$and (2.01±0.79) $\times10^{-6}$, respectively. They are comparable with those reported in literatures when the reaction conditions are concerned [5, 6, 19]. However, the RH typically varies from 20 % to 90 % in the real troposphere. As found in this work, the $\gamma_{t,ini}$ decreased exponentially with RH. Therefore, the γ_t measured under dry condition should overestimate the uptake ability of mineral dust to NO_2. Using the measured $\gamma_{t,ini}$ in the RH range of 32 %-74 %, we recommend that the $\gamma_{t,ini}$ of NO_2 on kaolin is (4.42±1.17) $\times10^{-8}$ at ambient RH, and it is (2.83±0.84) $\times10^{-7}$ on hematite. These values are slightly larger than the value recommended by Crowley et al [21]. According to the model results, it requires the $\gamma_{t,ini}$ being greater than 10^{-4} to observe an appreciable impact on NO_x and O_3 concentrations for the interactions of NO_2 with mineral dust [5]. Thus, the small uptake coefficients measured at ambient RH in this work imply that heterogeneous reactions of NO_2 on mineral dust might be unimportant for NO_x and O_3 concentrations. At present date, secondary inorganic aerosol (SIA) has attracted much attention in China's air pollution because SIA often abruptly increased in severe haze days [15-17]. The role of heterogeneous reaction in SIA formation has been confirmed in both field measurements, laboratory and modeling studies. As the typical RH was often varied in the range of 40%-80% in haze days in China [15], the influence of RH dependent kinetics on particulate species formation need to be evaluated with modeling studies in the future.

As a daytime source of OH radical, HONO formation attracts much attention. In this work, uptake of NO_2 at steady state was found mainly related to HONO formation. Similar to the recommended $\gamma_{t,ini}$ at ambient RH, we also recommend the $\gamma_{t,ss}$ of NO_2 at ambient RH to be (3.52±0.87) $\times10^{-9}$ and (1.35±0.14) $\times10^{-8}$ on kaolin and hematite, respectively. The corresponding HONO yield is (36.0±16.1) % and (75.9±3.32) %. Thus, the uptake coefficient for HONO formation at steady state ($\gamma_{t,ss,HONO}$) was calculated to be (1.27±0.88) $\times10^{-9}$ and (1.02±0.15) $\times10^{-8}$ on kaolin and hematite, respectively. Assuming the tropospheric concentration of NO_2 from 10 ppb to 50 ppb [42] and that of mineral dust from 40 $\mu m^2 \cdot cm^3$ to 150 $\mu m^2 \cdot cm^3$ with a fraction of hematite 6 % [13, 43], the possible formation rate of HONO via the reaction of NO_2 on hematite in mineral dust varies from 4.8×10^4 to 9.0×10^5 molecules$\cdot cm^3 \cdot day^{-1}$ using the estimated $\gamma_{t,ss,HONO}$ of hematite. Even if the $\gamma_{t,ss,HONO}$ of mineral dust is equal to that of hematite, the formation rate of HONO is estimated to be from 8.0×10^5 to 1.5×10^7 molecules$\cdot cm^3 \cdot day^{-1}$. This value is much lower than that on soot sample [4]. Therefore, the contribution of heterogeneous reaction of NO_2 on mineral dust to tropospheric HONO might be negligible under typical atmospheric conditions. However, the mass loading of dust often increased in severe haze days [44]. An et al. [45] have found that heterogeneous reaction significantly enhance concentrations of HONO and other particulate species in the North China Plain. It means more comprehensive modeling studies based upon our kinetics should be required to fully evaluate the role of HONO formation from heterogeneous reactions on dust in regional air quality. Additionally, the kinetic data is measured in the dark in this work. It is needed to investigate in the future whether the irradiation has enhancement effect on these reactions like that on Saharan sands [23].

Acknowledgements

This research was financially supported by the Strategic Priority Research Program of the Chinese Academy of Sciences (XDB05010300) and National Natural Science Foundation of China (51221892)

References

1. F. Arens, L. Gutzwiller, U. Baltensperger, H. W. Gaggeler and M. Ammann, *Environ. Sci. Technol.*, 2001, **35**, 2191-2199.
2. M. S. Salgado and M. J. Rossi, *Int. J. Chem. Kinet.*, 2002, **34**, 620-631.
3. J. McCabe and J. P. D. Abbatt, *J. Phys. Chem. C*, 2009, **113**, 2120-2127.

4. M. E. Monge, B. D'Anna, L. Mazri, A. Giroir-Fendler, M. Ammann, D. J. Donaldson and C. George, *Proc. Natl. Acad. Sci. USA.*, 2010, **107**, 6605-6609.
5. G. M. Underwood, C. H. Song, M. Phadnis, G. R. Carmichael and V. H. Grassian, *J. Geophys. Res.-Atmos.*, 2001, **106**, 18055-18066.
6. M. M. Angelini, R. J. Garrard, S. J. Rosen and R. Z. Hinrichs, *J. Phys. Chem. A*, 2007, **111**, 3326-3335.
7. H. J. Li, T. Zhu, D. F. Zhao, Z. F. Zhang and Z. M. Chen, *Atmos. Chem. Phys.*, 2010, **10**, 463-474.
8. Y. Bedjanian and A. El Zein, *J. Phys. Chem. A*, 2012, **116**, 1758-1764.
9. R. Vogt and B. J. Finlayson-Pitts, *J. Phys. Chem.*, 1994, **98**, 3747-3755.
10. D. D. Weis and G. E. Ewing, *J. Phys. Chem. A*, 1999, **103**, 4865-4873.
11. A. L. Goodman, G. M. Underwood and V. H. Grassian, *J. Phys. Chem. A*, 1999, **103**, 7217-7223.
12. A. Indarto, *Res. Chem. Intermediat.*, 2012, **38**, 1029-1041.
13. F. J. Dentener, G. R. Carmichael, Y. Zhang, J. Lelieveld and P. J. Crutzen, *J. Geophys. Res.* , 1996, **101**, 22869-22889.
14. Y. Zhang and G. Carmichael, *J Appli. Meteor.* , 1999, **38**, 353-366.
15. G. J. Zheng, F. K. Duan, H. Su, Y. L. Ma, Y. Cheng, B. Zheng, Q. Zhang, T. Huang, T. Kimoto, D. Chang, U. Pöschl, Y. F. Cheng and K. B. He, *Atmos. Chem. Phys.*, 2015, **15**, 2969-2983.
16. B. Zheng, Q. Zhang, Y. Zhang, K. B. He, K. Wang, G. J. Zheng, F. K. Duan, Y. L. Ma and T. Kimoto, *Atmos. Chem. Phys. Discuss.*, 2015, **15**, 2031-2049.
17. H. He, Y. Wang, Q. Ma, J. Ma, B. Chu, D. Ji, G. Tang, C. Liu, H. Zhang and J. Hao, *Sci. Rep.*, 2014, **4**.
18. M. Ndour, B. D'Anna, C. George, O. Ka, Balkanski, K. Y., S. J. and A. K., M.,, *Geophys. Res. Lett.*, 2008, **35**, L05812. doi:05810.01029/02007GL032006.
19. G. M. Underwood, T. M. Miller and V. H. Grassian, *J. Phys. Chem. A* 1999, **103** 6184-6190.
20. http://www.iupac-kinetic.ch.cam.ac.uk/.
21. J. N. Crowley, M. Ammann, R. A. Cox, R. G. Hynes, M. E. Jenkin, A. Mellouki, M. J. Rossi, J. Troe and T. J. Wallington, *Atmos. Chem. Phys.*, 2010, **10**, 9059-9223.
22. R. J. Gustafsson, A. Orlov, P. T. Griffiths, R. A. Cox and R. M. Lambert, *Chem. Commun.*, 2006, **37**, 3936-3938.
23. M. Ndour, M. Nicolas, B. D'Anna, O. Ka and C. George, *Phys. Chem. Chem. Phys.*, 2009, **11**, 1312-1319.
24. P. K. Mogili, P. D. Kleiber, M. A. Young and V. H. Grassian, *J. Phys. Chem. A*, 2006, **110**, 13799-13807.
25. Y. Liu, Q. Ma and H. He, *Atmos. Chem. Phys.*, 2009, **9**, 6273-6286.
26. L. Wang, W. Wang and M. Ge, *J. Environ. Sci.,* 2012, **24**, 1759-1766.
27. Z. Zhang, J. Shang, T. Zhu, H. Li, D. Zhao, Y. Liu and C. Ye, *J. Environ. Sci.* 2012, **24**, 1753-1758.
28. C. E. Kolb, R. A. Cox, J. P. D. Abbatt, M. Ammann, E. J. Davis, D. J. Donaldson, B. C. Garrett, C. George, P. T. Griffiths, D. R. Hanson, M. Kulmala, G. McFiggans, U. P¨oschl, I. Riipinen, M. J. Rossi, Y. Rudich, P. E. Wagner, P. M. Winkler, D. R. Worsnop and C. D. O. Dowd, *Atmos. Chem. Phys.* , 2010, **10**, 10561-10605.
29. Q. Ma, Y. Liu and H. He, *J. Phys. Chem. A*, 2008, **112**, 6630-6635.
30. C. Liu, Q. Ma, Y. Liu, J. Ma and H. He, *Phys. Chem. Chem. Phys.* , 2012, **14**, 1668-1676.
31. J. Baltrusaitis, P. M. Jayaweera and V. H. Grassian, *Phys. Chem. Chem. Phys.*, 2009, **11**, 8295-8305.
32. R. Wagner, T. Ajtai, K. Kandler, K. Lieke, C. Linke, T. Müller, M. Schnaiter and M. Vragel, *Atmos. Chem. Phys.*, 2012, **12**, 2491-2512.
33. C. Han, Y. Liu and H. He, *Environ. Sci Technol.*, 2013, **47**, 3174-3181.
34. D. O. Cooney, S.-S. Kim and E. J. Davis, *Chem. Eng. Sci.*, 1974, **29**, 1731-1738.
35. D. M. Murphy and D. W. Fahey, *Anal. Chem.*, 1987, **59**, 2753-2759.
36. V. H. Grassian, *Int. Rev. Phys. Chem.*, 2001, **20**, 467-548.
37. B. C. Hixson, J. W. Jordan, E. L. Wagner and H. M. Bevsek, *J. Phys. Chem. A*, 2011, **115**, 13364-13369.
38. C. R. Usher, A. E. Michel and V. H. Grassian, *Chem. Rev.*, 2003, **103**, 4883-4939.
39. S. Seisel, Y. Lian, T. Keil, M. E. Trukhin and R. Zellner, *Phys. Chem. Chem. Phys.,* 2004, **6**, 1926-1932.
40. J. C. Miranda-Trevino1 and C. A. Coles, *Appl. Clay Sci.*, 2003, **23**, 133-139.
41. C. D. Mashburn, E. K. Frinak and M. A. Tolbert, *J. Geophys. Res.*, 2006, **111**, D15213.
42. P. Wei, Z. Ren, F. Su, S. Cheng, P. Zhang and Q. Gao, *Acta Meteorol. Sin.*, 2011, **25**, 797-811.
43. Y. Liu, J. Ma and H. He, *Atmos. Chem. Phys.*, 2010, **10**, 10335-10344.
44. Minghui Tao, L. Chen, Lin Su and J. Tao, *J. Geophy. Res. Atmos.*, 2012, **117**, doi:10.1029/2012JD017915.
45. J. An, Y. Li, Y. Chen, J. Li, Y. Qu and Y. Tang, *Adv. Atmos. Sci.*, 2013, **30**, 57-66.